RSC Advances

PAPER

View Article Online
View Journal | View Issue

Cite this: *RSC Adv.*, 2024, **14**, 30127

Establishing a productive heterogeneous catalyst based on silver nanoparticles supported on a crosslinked vinyl polymer for the reduction of nitrophenol†

Y. A. Aggour,[a] El-Refaie Kenawy,[b] Marwa Magdy[a] and Elsayed Elbayoumy *[a]

The treatment of toxic nitrophenols in industrial wastewater is urgently needed from environmental, health, and economic points of view. The current study addresses the synthesis of the crosslinked vinyl polymer poly(acrylonitrile-*co*-2-acrylamido-2-methylpropane sulfonic acid) (poly(AN-*co*-AMPS)) through free radical copolymerization techniques using acrylonitrile (AN) and 2-acrylamido-2-methylpropane sulfonic acid (AMPS) monomers with different ratios and potassium persulfate (KPS) as an initiator in an aqueous medium. The prepared copolymer was utilized as a supporting matrix for silver nanoparticles (AgNPs) *via* the chemical reduction of silver nitrate within the copolymer framework. Different techniques were employed to characterize the prepared poly(AN-*co*-AMPS) and Ag/poly(AN-*co*-AMPS) composites, such as Fourier transform infrared (FTIR) spectroscopy, thermal gravimetric analysis (TGA), X-ray diffraction (XRD), transmission electron microscopy (TEM), and Brunauer–Emmett–Teller (BET) analysis. The results exhibit that silver metal was excellently dispersed across the surface of poly(AN-*co*-AMPS) without any agglomeration, presenting as nanocrystals with an average particle size equal to 6.21 nm. Also, BET analysis confirmed that the Ag/poly(AN-*co*-AMPS) composite exhibits mesoporous characteristics with a surface area of 59.615 $m^2\ g^{-1}$. Moreover, the Ag/poly(AN-*co*-AMPS) composite was effectively applied as a heterogeneous catalyst for the catalytic reduction of hazardous 4-nitrophenols (4-NP) with a rate constant equal to 0.28 min^{-1} and half-life time equal to 2.47 min to a less toxic compound in the presence of $NaBH_4$ as a reductant. Furthermore, the reusability experiment confirmed the excellent stability of Ag/poly(AN-*co*-AMPS). The catalyst can be easily separated from the reaction mixture using a simple centrifuge and directly reused for up to four successive cycles without a remarkable decrease in its catalytic activity. The conversion percentage of 4-NP after the four cycles was found to be 93%.

Received 17th July 2024
Accepted 7th September 2024

DOI: 10.1039/d4ra05186f

rsc.li/rsc-advances

1. Introduction

Due to the rapid increase in industry and modern technological applications, many organic compounds play an important and vital role in the production of valuable products.[1,2] Among these organic molecules, 4-NP, a simple aromatic compound, is a raw material used in numerous industries including the textile, paper, dye, explosive, petroleum, pesticide, drug, and pharmaceutical industries.[3–6] As a results, tons of hazardous and poisonous compounds as well as other side products are accumulated in the environment and cause harmful impacts on both humans and animals.[1–7] Because 4-NP is toxic, carcinogenic and highly soluble in water, it is considered to be one of the main reasons for water pollution and leads to many diseases.[8] These diseases including headaches, drowsiness, nausea, cyanosis, chest and stomach pain, kidney and liver damage, inflammation and disorders of central nervous system.[9–15] In addition, it is considered to be a main reason for various animals' mortal diseases.[16–18] Therefore, finding a solution for the problems associated with hazardous 4-NP is considered to be a critical research point and has attracted great interest in recent years. However, the presence of hazardous nitrophenol in water could be eliminated by numerous methods such as hydrogenation,[19,20] catalytic amination, photocatalytic degradation,[21] adsorption,[22] ozonation,[23] biodegradation,[24] and electrochemical techniques.[25] These methods suffer from some drawbacks, including long time consumption, high cost, low efficiency, strict conditions and the formation of toxic aromatic by-products.[26,27]

The chemical reduction of 4-NP to 4-aminophenol (4-AP) offers a safer and nontoxic strategy as well as being a promising

[a]*Chemistry Department, Faculty of Science, Damietta University, New Damietta 34517, Egypt. E-mail: sayedelbayoumy@du.edu.eg; yassina9@yahoo.com; marwasleem@du.edu.eg*

[b]*Polymer Research Group, Chemistry Department, Faculty of Science, Tanta University, Tanta 31527, Egypt. E-mail: ekenawy@yahoo.com*

† Electronic supplementary information (ESI) available. See DOI: https://doi.org/10.1039/d4ra05186f.

method with a short reaction time, low cost, and complete reduction efficiency compared with the other mentioned methods.[28] Because of the high surface-area-to-volume ratio of metal nanoparticles and their distinct physical and chemical properties, which are different from those of the bulk materials, they are applied and exhibit a vital role in different fields,[29,30] including catalysis, medicine, antiseptics, pharmaceutical agents, cosmetics, sensors, antimicrobial paints, photonics, renewable energy, magnetic devices, disinfectants and printable electronics.[31–33] To effectively catalyze hazardous organic molecules, various metal nanoparticles, such as silver, iron copper, palladium, nickel, cobalt, gold and platinum have been used.[34–42] Although AgNPs have high surface energy and surface area, non-toxicity, excellent electrical and thermal conductivity and high catalytic activity and reactivity,[43] they cannot be used alone in the catalytic reduction of nitrophenols due to the agglomeration process, which causes a decrease in their catalytic performance and surface area that leads to diminished efficiency of their catalytic process.[44,45]

Overall, loading AgNPs onto supporting materials such as polymers or surfactants enhances their stability, size distribution, and surface properties, and prevents aggregation.[46–48] Numerous polymers are used as a supporting material for AgNPs and as heterogenous catalysts. For instance, poly(2-isopropenyl-2-oxazoline-*co*-*N*-vinylpyrrolidone) was utilized as a stabilizing agent for AgNPs, which make them more stable for catalytic reaction.[33] AgNPs were also immobilized into poly(vinyl pyrrolidone-*co*-acrylic acid) as a supporting matrix and applied for the reduction of toxic 4-NP.[18] In addition, AgNPs were loaded into poly(*N*-isopropylacrylamide-*co*-acrylamide), and this hybrid system was used as a catalyst in some organic reaction transformations.[49] Moreover, AgNPs were stabilized in a β-1,4-poly-D-glucosamine modified graphite carbon electrode and used for the detection of 4-NP.[43] AgNPs were fabricated inside a poly(*N*-isopropylacrylamide-*co*-acrylic acid) hybrid microgel as a supporting material and used for *in vivo* reduction.[50] Furthermore, dispersed AgNPs were formed *in situ* on a ZrO_2 surface and used for the catalytic degradation of hazardous pollutants.[46] Amide-poly(methacrylic acid-*co*-acrylonitrile) was used as microreactors for the *in situ* synthesis of copper and cobalt nanoparticles for catalytic applications.[51] The synthesis and characterization of poly(acrylonitrile-*co*-2-acrylamido-2-methylpropane sulfonic acid) (poly(AN-*co*-AMPS)) has been reported by different authors,[52,53] but there are no reports on the production of AgNPs in this system or its application as a catalyst for the reduction of 4-NP. In the present study, we prepared a vinyl copolymer, poly(acrylonitrile-*co*-2-acrylamido-2-methylpropane sulfonic acid) (poly(AN-*co*-AMPS)), containing amide groups that are able to coordinate and act as a supporting material for AgNPs through two main steps as presented in Fig. 1. The first is the synthesis of poly(AN-*co*-AMPS) through the free radical copolymerization of AN and AMPS monomers, with KPS as an initiator and water as the solvent, while the second step is to load AgNPs on the surface of the prepared copolymer. Poly(AN-*co*-AMPS) has a high surface area and pore volume, which increase its ability to reduce toxic nitrophenols. In addition, it has high catalytic activity toward the reduction of 4-NP compared with another catalyst reported in the literature. Characterization of the copolymer and Ag copolymer nanocomposite were performed using FTIR, UV-visible, TGA, XRD, EDX, TEM and BET methods of analysis. Moreover, the catalytic activity of Ag/poly(AN-*co*-AMPS) toward the catalytic reduction of hazardous 4-NP to less toxic 4-AP is explored.

2. Materials and methods

2.1. Materials

Acrylonitrile (AN) monomer was purchased from Rasayan Laboratories. 2-Acrylamido-2-methylpropane sulfonic acid (AMPS, purity >98%) monomer was obtained from Fluka.

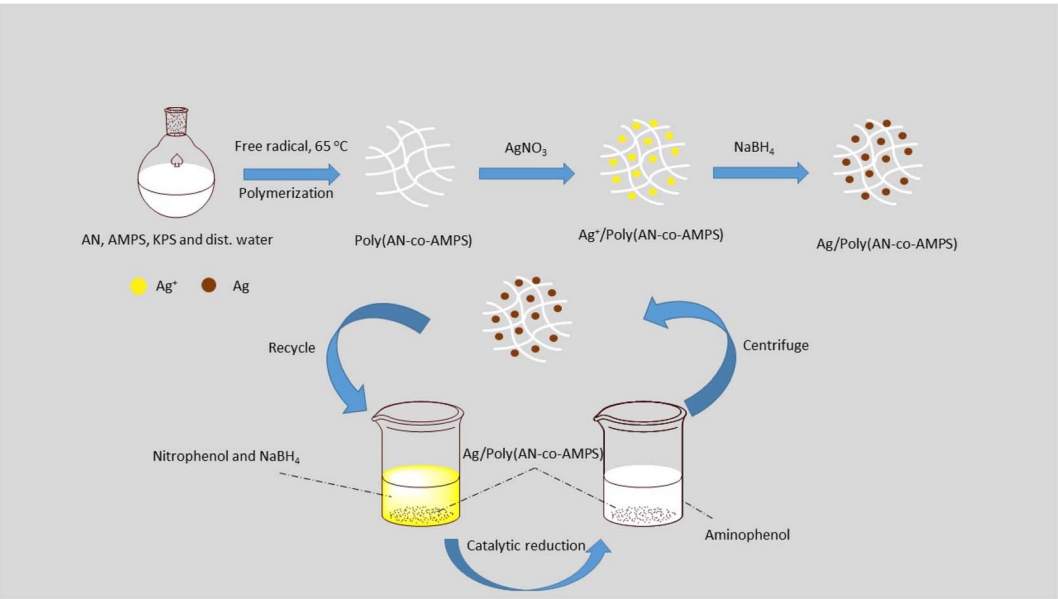

Fig. 1 Synthesis of Ag/poly(AN-*co*-AMPS) as a heterogenous catalyst for the catalytic reduction of 4-nitrophenol to 4-aminophenol.

Potassium persulfate (KPS) initiator was purchased from LOBA Chemie. 4-Nitrophenol (4-NP) and silver nitrate ($AgNO_3$) were received from Sigma-Aldrich. Sodium borohydride ($NaBH_4$) was obtained from Wako Chemical. Methanol (MeOH) with a high grade was received from a commercial source. All chemicals were used as received without any further purifications.

2.2. Synthesis of poly(AN-*co*-AMPS)

Poly(AN-*co*-AMPS) was synthetized according to free radical copolymerization techniques using AN and AMPS as monomers with different ratios and KPS as an initiator.[54] For example, the synthesis of poly(AN-*co*-AMPS) in run 1 in Table 1 was as follows. AMPS monomer (0.414 g, 2 mmol), AN (5.194 g, 98 mmol), and KPS (0.056 g, 0.21 mmol) were added to a 100 mL round bottom flask containing distilled water (60 mL) as a solvent. The reaction mixture was stirred until the formation of a homogeneous solution occurred. After that, the reaction mixture was heated at 65 °C with continuous stirring for 4 h. The obtained white precipitate of the copolymer was collected by filtration, followed by washing with distilled water to remove any remaining initiator or unreacted monomers. Finally, the prepared copolymer was dried under vacuum until its weight became constant, and the obtained yield was 5 g (89.15%) of poly(AN-*co*-AMPS) as a white solid powder.

2.3. Synthesis of silver nanoparticle–polymer composite

Silver nanoparticles (AgNPs) were loaded within the framework of poly(AN-*co*-AMPS) by immersing the polymer in a solution of silver nitrate, followed by reduction using a freshly prepared $NaBH_4$ solution.[32,55] In detail, poly(AN-*co*-AMPS) (0.5 g) was added to 20 mL of methanol containing x grams of $AgNO_3$ (where $x = 0.016, 0.033, 0.05, 0.069, 0.087$ g), and the resulting suspension was stirred for 2 h to ensure that the Ag ions were deeply loaded into the poly(AN-*co*-AMPS) framework. After that, the resulting Ag^+/poly(AN-*co*-AMPS) complexes with different amounts of Ag^+ equal to 2, 4, 6, 8, 10% of copolymer weight were filtered out and washed with methanol several times to remove any unloaded $AgNO_3$ from the copolymers. To each of the obtained Ag^+/poly(AN-*co*-AMPS) complexes, 5 mL of a freshly prepared methanol solution of $NaBH_4$ (0.096 g, 507.53 mM) was added dropwise with stirring for another 1 h, and the reaction mixture color changed from white to brown, indicating the reduction of Ag^+ to Ag^0 along the polymeric chain. Finally, the obtained Ag/poly(AN-*co*-AMPS) nanocomposites were filtered, washed with methanol, dried, and kept for further studies.

2.4. Catalytic reduction of nitrophenol

The prepared silver nanocomposites Ag/poly(AN-*co*-AMPS) were used for the reduction of 4-NP to 4-AP in an excess amount of $NaBH_4$ as a model reaction in order to investigate their catalytic activities. For this purpose, 5 mL of an $NaBH_4$ aqueous solution (100 mM) was mixed with 5 mL of a 4-NP aqueous solution (1 mM). The reaction mixture was completed to 50 mL with distilled water, and then 20 mg of Ag/poly(AN-*co*-AMPS) was added as a catalyst. The reduction process was carried out at room temperature and was monitored at regular time intervals by measuring the absorption peak of 4-NP at 400 nm using UV-vis spectroscopy.

2.5. Characterization techniques

FTIR spectra were measured in the scanning range 4000–400 cm^{-1} with a JASCO FT/IR-6100 spectrometer using a KBr pellet sample. Thermal gravimetric analysis (TGA) was carried out on a Rigaku Thermo plus TG8120 instrument under a nitrogen atmosphere at a heating rate of 10 K min^{-1} with a flow rate of 20 mL min^{-1} using an aluminum crucible from room temperature to 800 °C. X-ray diffraction (XRD) was performed using a Siemens D-500 X-ray diffractometer ($\lambda = 1.54$ Å (Cu Kα)). Transmission electron microscopy (TEM) images were obtained using a Model Talos L120C G2 TEM, ThermoFisher, Europe. Scanning electron microscopy (SEM) was conducted using a JEM-2100F microscope at an accelerating voltage of 200 kV. The Brunauer–Emmett–Teller (BET) method was applied to determine surface area and pore volume by nitrogen sorption using a Quantachrome instrument (USA). A Jasco V-630 UV-visible automatic recording spectrophotometer was used to record the UV-vis absorption spectra at room temperature using solution in a 1 cm quartz cell at a wavelength range of 250 to 500 nm.

3. Results and discussion

3.1. FTIR analysis

The FTIR spectra of the poly(AN-*co*-AMPS) and Ag/poly(AN-*co*-AMPS) nanocomposites are shown in Fig. 2. Starting with poly(AN-*co*-AMPS), the characteristic peaks at 1041.4 cm^{-1}, 1449.2 cm^{-1}, 1562 cm^{-1} are attributed to the stretching vibration of S=O in the sulfonic acid group, the bending vibration of C–H, and the bending vibration of the N–H group, respectively.[53] The two specific peaks at 1652.7 cm^{-1} and 2245.7 cm^{-1} are related to the stretching vibrations of C=O[56] and the nitrile

Table 1 Synthesis of p(AN-*co*-AMPS) by free radical polymerization using KPS as an initiator at 65 °C for 4 h[a]

Run	Copolymer	M_1	M_2	M_1 (mmol)	M_2 in feed	Yield (%)	S content[b] (%)	M_1/M_2 in copolymer[c]
1	Poly(AN-*co*-AMPs)-1	AN	AMPS	98	2	89.15	0.21	98.6/1.4
2	Poly(AN-*co*-AMPs)-2	AN	AMPS	95.7	4.3	68.4	0.36	97.7/2.3
3	Poly(AN-*co*-AMPs)-3	AN	AMPS	92	8	56.18	0.88	94.3/5.7

[a] $M_1 = 5.194$ g, $M_2 = 0.414$ g (run 1); $M_1 = 5.072$ g, $M_2 = 0.89$ g (run 2); $M_1 = 4.876$ g, $M_2 = 1.656$ g (run 3); solvent: distilled water; KPS = (0.056 g, 0.21 mmol). [b] Determined from EDX analysis (Fig. S1 in ESI). [c] Determined from the percentage of S atoms in the copolymer.

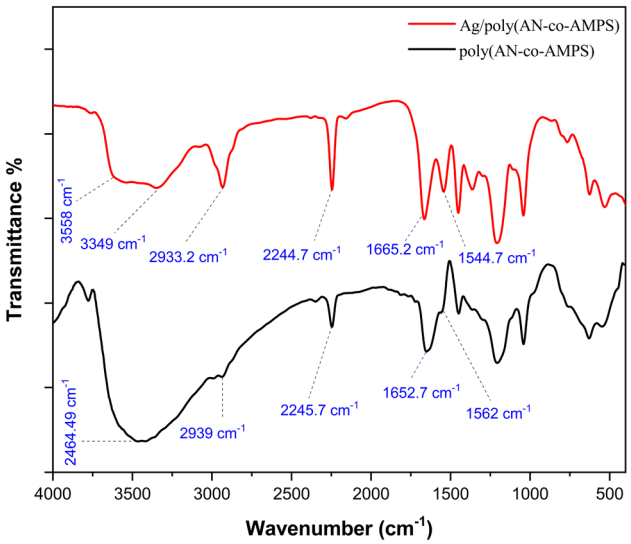

Fig. 2 FTIR spectra of poly(AN-*co*-AMPS) and Ag/poly(AN-*co*-AMPS).

group (C≡N),[57] respectively. In addition, the stretching vibration peaks at 2939 cm^{-1} and 2998.8 cm^{-1} are due to the symmetric and asymmetric stretching of C–H.[53] Furthermore, the broad peak at 3464.5 cm^{-1} is due to the NH and OH groups.[58] Moving on to the Ag/poly(AN-*co*-AMPS) composite, it exhibits the same peaks as poly(AN-*co*-AMPS); however, the two characteristic peaks of C=O and NH are shifted from 1652.7 cm^{-1} and 1562 cm^{-1} to appear at 1665.2 cm^{-1} and 1544.7 cm^{-1}, respectively. Also, the amide group band of Ag/poly(AN-*co*-AMPS) was cleaved into two bands appearing at 3558 cm^{-1} and at 3349 cm^{-1}; this change may be due to the interaction of the NH amide groups in poly(AN-*co*-AMPS) and AgNPs.[59] In addition, the amide bands of Ag/poly(AN-*co*-AMPS) are not as broad as for the copolymer. Moreover, the peaks of C=O and NH have lower intensity, indicating that the C=O and N–H vibrations were affected by the attachment of silver to the nitrogen from the copolymer.[59] This observation confirms the participation of the amide groups of the copolymer in the complexation of AgNPs within the framework of poly(AN-*co*-AMPS).[49]

3.2. Thermal gravimetric analysis

Thermal gravimetric analysis (TGA) was performed to investigate the thermal stability of poly(AN-*co*-AMPS), as shown in Fig. 3. According to the TGA curve of poly(AN-*co*-AMPS), two degradation stages are observed during the heating process, with different amounts of weight loss. The first degradation stage showed a slight decrease in weight starting from ambient temperature to 185 °C, accompanied by a weight loss percentage equal to 3.72%. The weight loss in this stage could be due to the loss of moisture or residual solvent from the copolymer matrices.[60] However, the second stage showed a higher degradation rate and a weight loss percentage equal to 49.04% in the temperature range 185–800 °C. This second degradation stage could be assigned to the decomposition of the polymer backbone chain.[55–60]

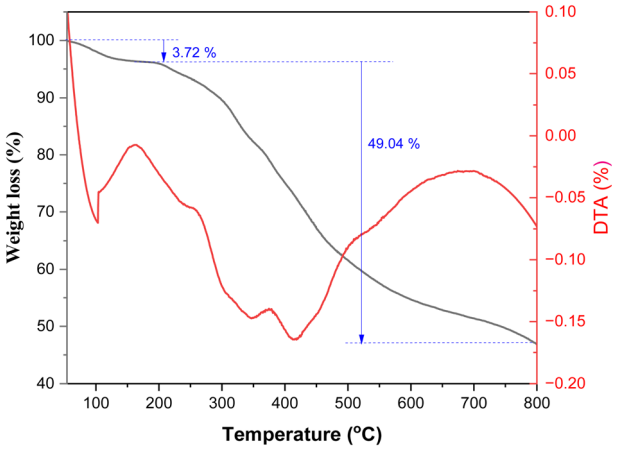

Fig. 3 TGA of poly(AN-*co*-AMPS).

The Coats–Redfern method was used to determine both the thermodynamic parameters and the activation energy of the main (second stage) thermal degradation stage for poly(AN-*co*-AMPS).[61,62] According to this method, the first-order reaction mathematical formula is given by eqn (1):

$$\log\left[\frac{-\log(1-\alpha)}{T^2}\right] = \log\left[\frac{A'R}{\theta E^*}\left(1-\frac{2RT}{E^*}\right)\right] - \frac{E^*}{2.303RT^*} \quad (1)$$

where E^* is the activation energy, θ is the heating rate, R is the universal gas constant, A' is the Arrhenius constant, and α is the fraction of the sample decomposed at temperature T, which can be determined according to eqn (2) below:

$$\alpha = \frac{W_o - W_t}{W_o - W_f} \quad (2)$$

where W_o is the original weight of sample, W_t is weight of the sample at temperature T and W_f is the final weight of the sample at the end of the reaction. By applying eqn (1) to the experimental TGA data and plotting $\log(-\log(1-\alpha)/T^2)$ against $1/T$, a straight line was produced (Fig. S2 in the ESI†). The values of E^* were calculated from the slope, and the A' value was calculated from the intercept.

Eqn (3)–(5) were used to determine the enthalpy (ΔH^*), entropy (ΔS^*) and change in free energy (ΔG^*) of the activation for the degradation process.[63]

$$\Delta H^* = E^* - RT \quad (3)$$

$$\Delta S^* = 2.303R\left[\log\left(\frac{A'\hbar}{K_B T}\right)\right] \quad (4)$$

$$\Delta G^* = \Delta H^* - T\Delta S^* \quad (5)$$

where $\hbar$ is the Planck constant and K_B is the Boltzmann constant. Table 2 presents the activation energy, Arrhenius constant, and thermodynamic parameters for poly(AN-*co*-AMPS). The positive values of ΔG^* and ΔH^* indicate that the degradation of copolymer is a nonspontaneous and endothermic process, respectively.

Table 2 Thermodynamic parameters of poly(AN-*co*-AMPS)

Polymer	E^* (kJ mol^{-1})	A' (min^{-1})	ΔS^* (J mol^{-1} K^{-1})	ΔH^* (kJ mol^{-1})	ΔG^* (kJ mol^{-1})
Poly(AN-*co*-AMPS)	30.846	7.2	−568.5	25.126	416.25

3.3. XRD analysis

XRD analysis was performed to investigate the crystalline structure of the prepared Ag/poly(AN-*co*-AMPS) copolymer nanocomposite, and the results are presented in Fig. 4 and Table 3. As shown in Fig. 4, the XRD patterns of poly(AN-*co*-AMPS) and Ag/poly(AN-*co*-AMPS) exhibit two characteristic peaks at $2\theta = 17.039°$ and 29.381°, which were assigned to the crystalline structure of poly(AN-*co*-AMPS).[64,65] In addition, four sharp characteristic peaks are produced at $2\theta = 38.066°$, 43.939°, 64.315° and 77.314°, which were attributed to the (111), (200), (220) and (311) sets of lattice planes, respectively. These four characteristic peaks are highly matched with the ICSD reference code 01-071-4613, confirming the presence of crystalline AgNPs within the copolymer chain. The crystallite size (D) of the prepared Ag/poly(AN-*co*-AMPS) copolymer nanocomposite was calculated using the well-known Scherrer eqn (6) below:[66]

$$D = \frac{K\lambda}{\beta \cos(\theta)}, \quad (6)$$

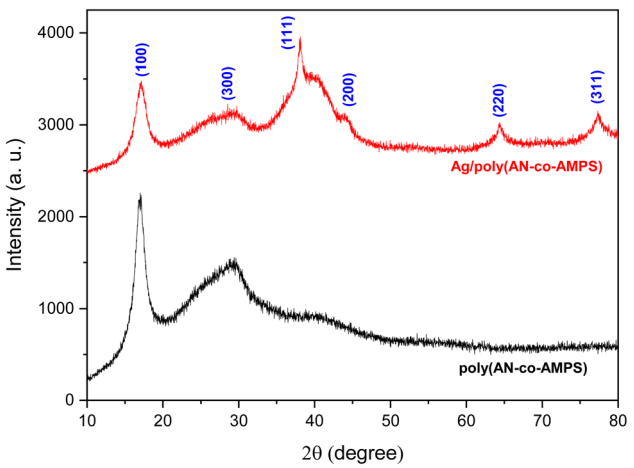

Fig. 4 XRD patterns of poly(AN-*co*-AMPS) and Ag/poly(AN-*co*-AMPS).

where K is Scherrer's constant ($K = 0.89$), λ is the X-ray radiation wavelength ($\lambda = 0.154$ nm), β is the full width at half-maximum intensity (FWHM) and 2θ is Bragg's angle (peak position). After applying this equation to the main peak corresponding to the AgNPs, we were able to determine their average crystallite size, which was found to be equal to 1.45 nm.

3.4. TEM and SEM analysis

The size and morphology of the AgNPs immobilized in poly(AN-*co*-AMPS) were investigated using TEM analysis, as shown in Fig. 5. As shown in the figure, the poly(AN-*co*-AMPS) did not exhibit any specific shape, and the AgNPs were excellently dispersed through the copolymer network and appeared as dark spherical spots of silver nanoclusters. The particle size distribution of the AgNPs was estimated by measuring the diameter of more than 100 AgNPs obtained from the TEM images with the aid of the software ImageJ. The results indicate that the AgNPs have an average particle size equal to 6.21 nm. In addition, no clear agglomeration of AgNPs was observed in the copolymer network.

Scanning electron microscopy (SEM) was used to analyze the surface morphological and textural properties of poly(A-*co*-AMPS) and Ag/poly(A-*co*-AMPS). The resulting images are shown in Fig. 6. Our analysis revealed that poly(AN-*co*-AMPS) did not have a defined shape and was made up of irregularly shaped particles. It also revealed that the AgNPs were uniformly dispersed and exhibited a spherical shape.

3.5. Brunauer–Emmett–Teller (BET) analysis

BET surface area analysis was used to evaluate the specific surface area and pore volume of the Ag/poly(AN-*co*-AMPS) composite by using N_2 adsorption/desorption measurements at 77 K. The nitrogen adsorption/desorption isotherms of Ag/poly(AN-*co*-AMPS) are shown in Fig. 7. According to the BET results, the adsorption/desorption curves are a type-IV isotherm, and Ag/poly(AN-*co*-AMPS) has a specific surface area equal to 59.615 m^2 g^{-1}. Furthermore, the BJH pore radius and the BJH pore volume obtained at a saturated pressure were determined to be

Table 3 XRD data of Ag/poly(AN-*co*-AMPS)

No.	2θ (°)	d value (Å)	Miller indices	Net intensity (counts)	Relative intensity (%)
1	17.039	5.19957	(100)	616.741	72.1
2	29.381	3.03747	(300)	358.305	41.9
3	38.066	2.36209	(111)	855.777	100.0
4	43.939	2.05900	(200)	311.061	36.3
5	64.315	1.44726	(220)	195.317	22.8
6	77.314	1.23280	(311)	205.124	24.0

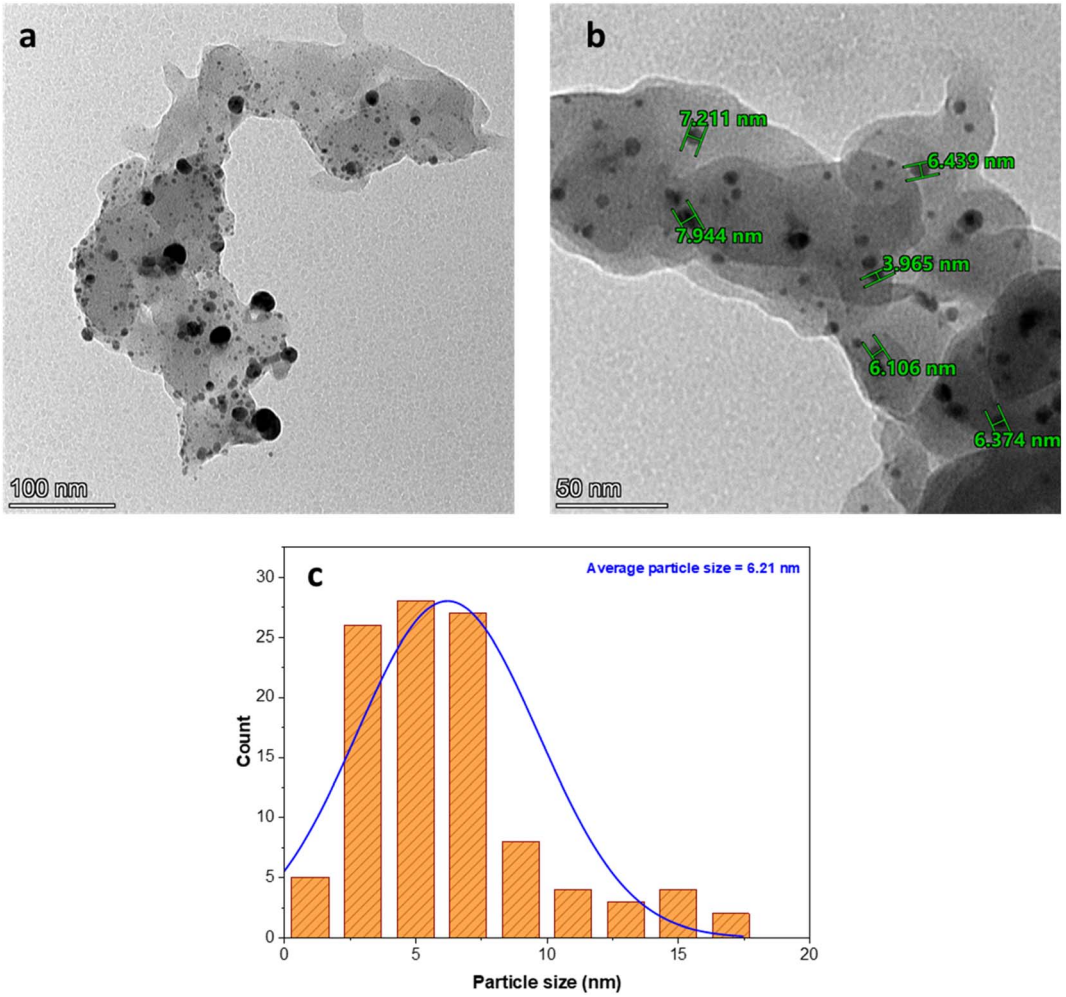

Fig. 5 TEM images (a and b) and particle size distribution (c) of the Ag/poly(AN-*co*-AMPS) composite.

8.826 nm and 0.358 $cm^3\ g^{-1}$, respectively. The International Union of Pure and Applied Chemistry (IUPAC) classifies porous materials based on their pore radius; microporous materials have a pore radius of less than 2 nm, mesoporous materials have a pore radius in the range of 2–50 nm and macro-porous materials have a pore radius greater than 50 nm.[67] Consequently, we can say that Ag/poly(AN-*co*-AMPS) is a mesoporous catalyst.

3.6. Catalytic activity of Ag/poly(AN-*co*-AMPS)

The catalytic performance of the prepared Ag/poly(AN-*co*-AMPS) nanocomposite was investigated using the reduction of 4-NP into 4-AP as a model reaction in the presence of $NaBH_4$ in an aqueous medium. Because both the reactant and product are sensitive to UV-visible light with different maximum absorbance wavelengths, the model reaction was monitored using a UV-visible spectrophotometer. Initially, we studied the effect of $NaBH_4$ (reductant) and poly(AN-*co*-AMPS) without any silver metal toward the reduction of 4-NP. The results indicated that neither $NaBH_4$ nor poly(AN-*co*-AMPS) has the ability to catalyze the reduction of 4-NP (Fig. S3 in ESI†). On the other hand, when Ag/poly(AN-*co*-AMPS) was used as the catalyst, the absorption peak intensity of 4-NP at 400 nm disappeared, and a new absorption peak at 300 nm corresponding to the product 4-AP was formed. Fig. 8A presents the UV-visible spectra of the catalytic reduction of 4-NP using Ag/poly(AN-*co*-AMPS) as a catalyst in the wavelength range of 250 nm to 500 nm. As shown in Fig. 8A, the absorption peak intensity at 400 nm, which corresponds to 4-NP, gradually decreases as the reaction time progresses, and the yellow color of 4-NP disappears after about 12 minutes. In addition, a new peak started to appear at 300 nm, confirming the formation of 4-AP.[35]

Moreover, our study was extended to explore the kinetic behavior of the catalytic reduction of 4-NP. Because $NaBH_4$ is consumed in an excess amount relative to the concentration of 4-NP, the pseudo-first order kinetic assumption is applied, and its mathematical equation is described below:

$$\ln\left(\frac{A_t}{A_0}\right) = -kt \quad (7)$$

where A_0 and A_t are the absorbance of 4-NP at 400 nm at time zero and at any time t, respectively. k is the reduction rate constant. Applying eqn (7) to the experimental data yields

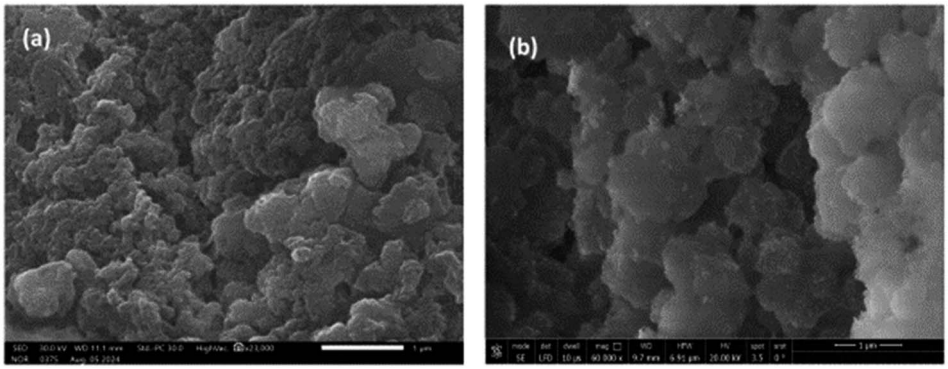

Fig. 6 SEM images of the poly(AN-*co*-AMPS) composite (a) and Ag/poly(AN-*co*-AMPS) composite (b).

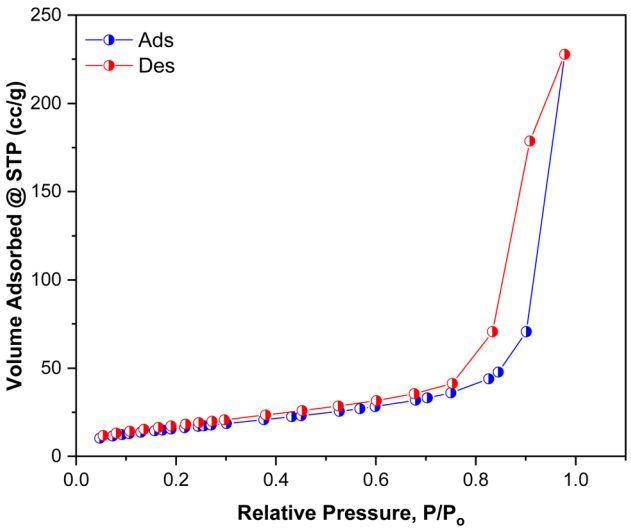

Fig. 7 N_2 adsorption–desorption isotherms of Ag/poly(AN-*co*-AMPS).

a straight-line with an R^2 value equal to 0.9609 (Fig. 8B), indicating that the reduction process has begun and follows pseudo-first order kinetics. The value of the rate constant was determined from the slope of the line and was found to be equal to 0.23681 min^{-1}. Furthermore, the half-life time ($t_{1/2}$) was determined from the value of k and was found to be 2.927 min.

In order to investigate the optimum conditions for the catalytic reduction of 4-NP, the effect of different variables, such as the ratio between the two monomers in the copolymer chain, amount of AgNPs on the catalyst, concentration of $NaBH_4$, and the amount of catalyst were studied, and the results are presented in Fig. 9. The dependence of the reaction rate (k) on the ratio of the two monomers in the polymer network is illustrated in Fig. 9a and Table 4. As can be seen, increasing the percentage of AMPS monomer from 1.4 to 5.7 leads to an increase in the value of k from 0.03 to 0.132 min^{-1} and a decrease in the value of $t_{1/2}$ from 23.11 to 5.25 min (Table 4). This behavior could be explained by the ability of the amide functional group in the AMPS moieties to interact with AgNPs, which leads to a good distribution of AgNPs throughout the copolymer framework. This interaction between amide groups and AgNPs was confirmed as mentioned above in the FTIR analysis of the copolymer and its silver composite.

Also, the k value of the catalytic reduction of 4-NP exhibits a strong dependence on the percentage of AgNPs present in the

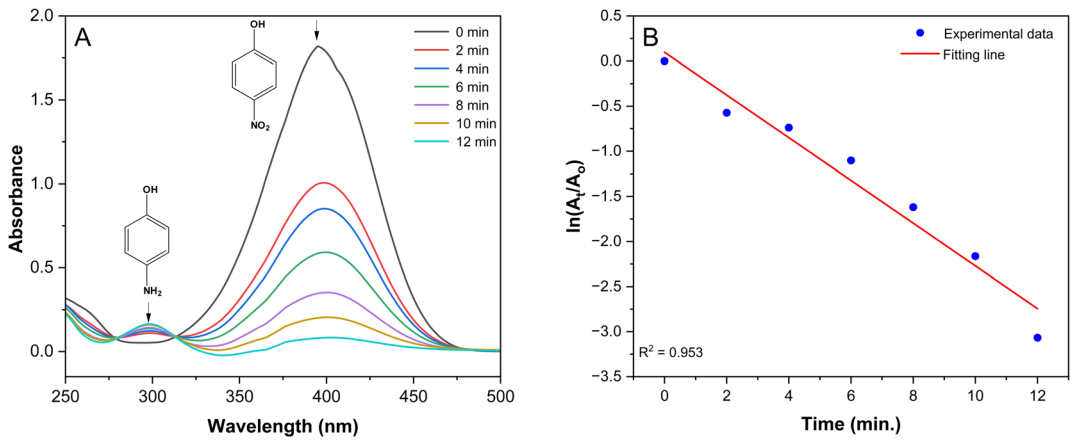

Fig. 8 UV-vis spectra of the reduction of 4-NP to 4-AP (A); pseudo-first-order reaction kinetics of the reduction of 4-NP to 4-AP (B). Reaction conditions: [4-NP] = 0.1 mM, [$NaBH_4$] = 10 mM, 20 mg catalyst containing 8% of AgNPs.

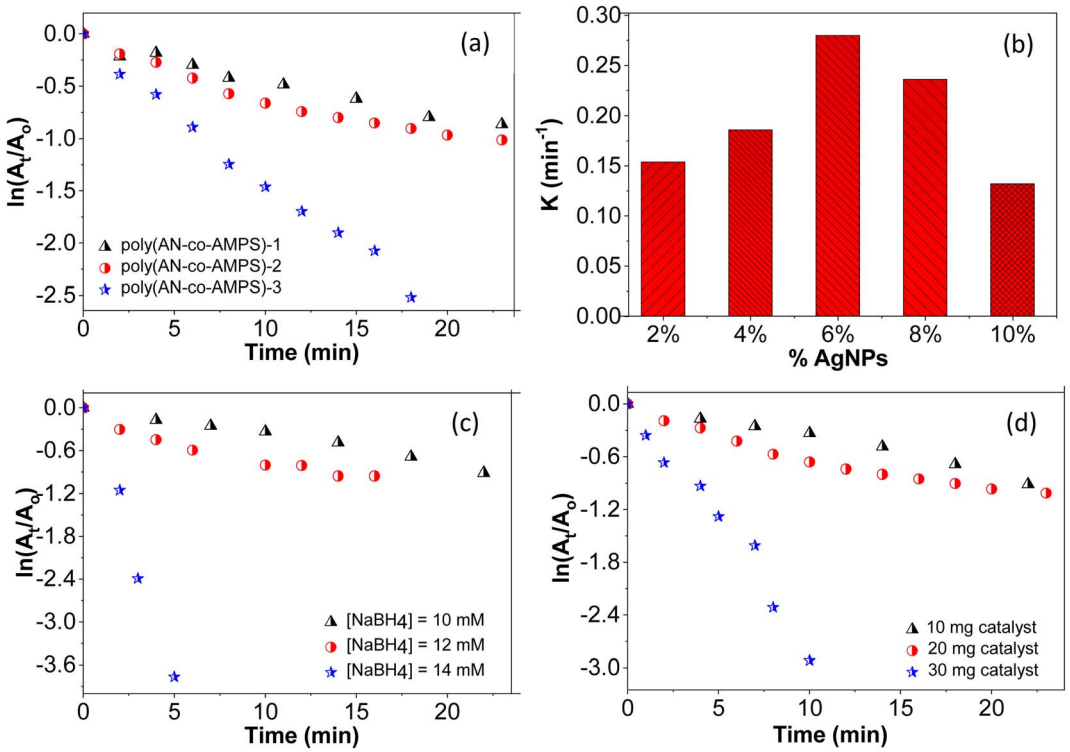

Fig. 9 (a) Dependance of the rate of catalytic reduction of 4-NP on the ratio of the two monomers. Reaction conditions: [4-NP] = 0.1 mM, [$NaBH_4$] = 10 mM, weight of catalyst = 20 mg. (b) Dependance of the rate of catalytic reduction of 4-NP on the percentage of AgNPs. Reaction conditions: [4-NP] = 0.1 mM, [$NaBH_4$] = 10 mM, weight of catalyst = 20 mg. (c) Dependance of the rate of catalytic reduction of 4-NP on the concentration of $NaBH_4$. Reaction conditions: [4-NP] = 0.1 mM, weight of catalyst = 10 mg; (d) dependance of the rate of catalytic reduction of 4-NP on the amount of catalyst. Reaction conditions: [4-NP] = 0.1 mM, [$NaBH_4$] = 10 mM.

catalyst framework. As illustrated in Fig. 9b and Table 4, the reaction rate gradually increases with increasing the amount of AgNPs up to 6%, at which the maximum value of k (0.28 min^{-1}) and the minimum value of $t_{1/2}$ (2.47 min) are observed. However, with increasing the amount of AgNPs beyond 6%, the opposite behavior was noted, and the reaction rate started to diminish, which reflected the decreasing value of k and increasing value of $t_{1/2}$. The reason for the increase in the value of k as the amount of AgNPs was increased up to 6% was attributed to the increased surface area of catalyst, which facilitates the catalytic reduction reaction.[68–71] Increasing the amount of AgNPs beyond 6% could lead to the agglomeration of

Table 4 Dependance of the rate constant and half-life time of the catalytic reduction of 4-NP to 4-AP on different variables

	Variables					
Run	AMPS (%) in copolymer	Wt% of AgNPs	[$NaBH_4$] (mM)	Catalyst wt. (mg)	k (min^{-1})	$t_{1/2}$ (min)
1	1.4				0.03	23.11
2	2.3	10	10	20	0.04	17.33
3	5.7				0.132	5.25
4		2			0.154	4.5
5		4			0.186	3.73
6	5.7	6	10	20	0.28	2.47
7		8			0.236	2.94
8		10			0.132	5.25
9			10		0.04	17.33
10	2.3	10	12	10	0.05	13.86
11			14		0.077	9
12				10	0.04	17.33
13	2.3	10	10	20	0.05	13.86
14				30	0.278	2.49

AgNPs, which would diminish the catalyst performance due to a reduction in the surface area available for catalyzing the reduction reaction.[7,18]

Fig. 9c shows the dependence of the reaction rate as the concentration of $NaBH_4$ is varied from 10 to 14 mM. The results demonstrate that increasing the concentration of $NaBH_4$ leads to an increase in the value of k and a decrease in the value of $t_{1/2}$ (Table 4). The reason for this observation can be regarded as the greater conversion of the reactants into their reduced form due to the greater availability of reducing agents in the reaction medium, which leads to increased reaction rate.[18,49]

Furthermore, the effect of catalyst dose on the rate of the reduction reaction was investigated by adding different amounts of catalyst in the range of 10–30 mg; the experimental results are presented in Fig. 9d. As shown in this figure, the rate of reduction increased with increasing the amount of catalyst. This could be due to an increase in the active surface sites available for reaction with 4-NP, which leads to an increase in the reduction reaction rate of 4-NP.[29,35]

3.7. Reaction mechanism

According to the Langmuir–Hinshelwood mechanism,[72,73] sodium borohydride functions as a hydrogen source. It ionizes in liquid phase, resulting in the production of borohydride ions (BH_4^-). The proposed mechanism of the catalytic reduction of 4-NP to 4-AP is illustrated in Fig. 10. Initially, BH_4^- ions and 4-NP are diffused and adsorbed into the surface of the catalyst. Subsequently, the positively charged hydrogen atom of BH_4^- forms electrostatic attractions with the negatively charged oxygen from the nitro groups of the 4-NP at the catalyst surface, making the removal of oxygen and reduction of the nitro groups easier. Furthermore, the residual nitrogen of $-NO_2$ is also negatively charged, so the H atoms of the positively charged H_2O molecules could combine easily with the residual nitrogen of nitrophenol followed by hydrodeoxygenation, and finally, the release of 4-AP from the surface of the catalyst. Electron transfer from the donor BH_4^- ions to 4-NP through the surface of the catalyst must occur simultaneously in addition to the proton transfer and deoxygenation to maintain charge balance and complete the reduction process.

3.8. Recyclability of the catalyst

After 4-NP had been completely reduced to 4-AP, the Ag/poly(AN-*co*-AMPS) catalyst was separated by centrifugation from the reaction solution, washed with methanol, dried at room temperature, and reused without any further pretreatment for a new cycle to investigate its catalytic stability. The results of the recycling experiment are shown in Fig. 11a. The results exhibit that there is no significant decrease in the efficiency of the conversion percentage of 4-NP after reuse for four successive cycles. These results confirm and prove the relative efficiency, stability, and durability of the catalyst under the experimental conditions. Also, XRD analysis of the catalyst before and after the recycling experiments is shown in Fig. 11b. This figure shows that the positions of the diffraction peaks and crystalline forms of Ag/poly(AN-*co*-AMPS) did not change after recycling for four cycles, which indicates the stability of the catalyst.

In order to evaluate the efficiency of the Ag/poly(AN-*co*-AMPS) catalyst, we compared its catalytic activity toward the reduction of 4-NP with that of other catalysts reported in the literature, and the data is collected in Table 5. Although direct comparison with the reported catalysts is difficult due to the variety of reaction conditions, such as the concentrations of 4-NP and $NaBH_4$ and the catalyst dose, the Ag/poly(AN-*co*-AMPS) catalyst

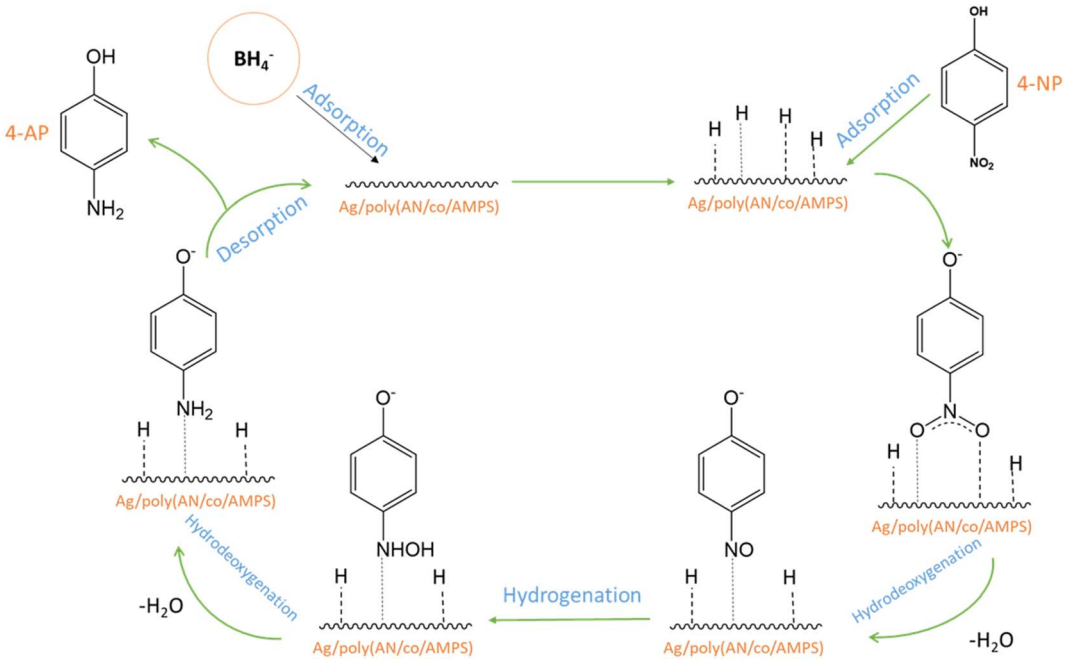

Fig. 10 Proposed mechanism for the catalytic reduction of 4-NP into 4-AP.

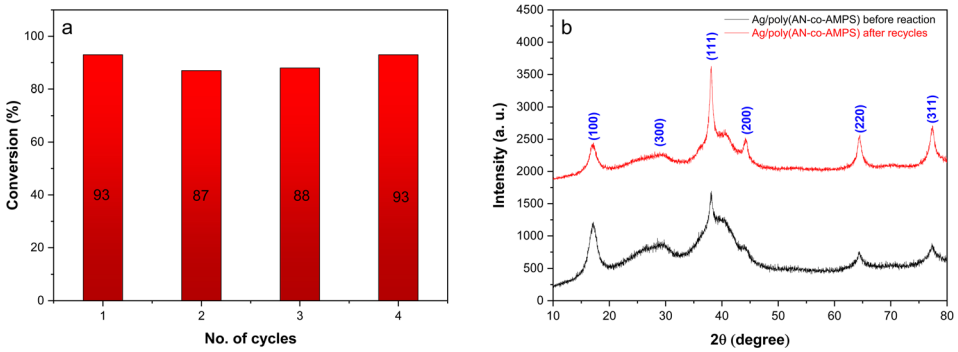

Fig. 11 (a) Recycling experiments for the catalytic reduction of 4-NP to 4-AP. Reaction conditions: [4-NP] = 0.1 mM, [$NaBH_4$] = 10 mM, weight of catalyst Ag/poly(AN-*co*-AMPS) = 20 mg and time = 12 min; (b) XRD analysis of Ag/poly(AN-*co*-AMPS) before and after the recycling experiments.

Table 5 Comparison of the catalytic reduction of 4-NP to 4-AP over various catalysts

		Reaction conditions				
No.	Catalyst	[4-NP] mM	[$NaBH_4$] mM	Wt. cat. mg	K (min^{-1})	Ref.
1	Ag/poly(AN-*co*-AMPS)	0.1	10	20	0.28	Present study
2	Ag–P(NIPAM-*co*-AAm)	0.06	9.15	23.90	0.281	49
3	PIPO*x*_PNVP-SNCs	1	50	100	0.486	33
4	Ag/poly(norepinephrine)/MnO_2	1	200	1	0.4644	71
5	Ag@chitosan	—	0.1	40	0.143	7
6	AuCu@Pt nanoalloys	1	100	0.1 mL	0.039	70
7	Pd–Ni/rGO	0.5	30	0.2	0.16	74
8	Pt–Ni nanoparticles	0.1	0.1	0.1	0.11	75
9	Starch-supported gold	1	15	100	0.0326	76

is regarded as one of the most active catalysts, exhibiting an advantage over the other catalysts showing similar activities in the aspects that it can be more readily prepared than the competitors and that it works at the lowest concentration of $NaBH_4$.

4. Conclusion

In this work, we have effectively synthesized an Ag/poly(AN-*co*-AMPS) nanocomposite, which serves as a versatile and effective heterogenous catalyst for the reduction of toxic nitrophenol. The results demonstrate that poly(AN-*co*-AMPS) effectively acts as a supporting matrix for AgNPs. Coordination with the amide group present in the copolymer framework allows the uniform dispersion of silver throughout the copolymer framework as silver nanoclusters with an average crystalline size of 1.576 nm, and its surface prevents the agglomeration of the silver. The reduction reaction of 4-NP was completed in 14 min and found to be pseudo-first-order with an apparent rate constant and half-life time equal to 0.28 min^{-1} and 2.47 min, respectively. Moreover, the catalyst can be removed from the reaction mixture *via* centrifugation and reused for four consecutive cycles with a slight decrease in its catalytic activity. Overall, this catalyst provides an efficient and practical way to remove hazardous organic compounds from industrial wastewater and produces aminophenol, which has potential applications as a raw material in many industries.

Data availability

The data that support the findings of this study are available from the corresponding author upon reasonable request.

Author contributions

Y. A. Aggour: supervision, project administration, conceptualization, resources, writing – review & editing; El-Refaie Kenawy: supervision, conceptualization, investigation, writing – review & editing; Marwa Magdy: investigation, data curation, calculation, visualization, formal analysis, methodology, writing – original draft; Elsayed Elbayoumy: supervision, conceptualization, validation, formal analysis, investigation, resources, data curation, writing – review & editing.

Conflicts of interest

The authors declare that they have no known competing financial interests or personal relationships that could have appeared to influence the work reported in this paper.

Acknowledgements

We thank the central laboratory at faculty of Science, Damietta university for providing the facilities to conduct UV-vis spectroscopy analysis.

References

1 A. Serrà, R. Artal, M. Pozo, J. Garcia-Amorós and E. Gómez, Simple environmentally-friendly reduction of 4-nitrophenol, *Catalysts*, 2020, **10**(4), 458.
2 E. M. Sitinjak, I. Masmur, N. V. M. D. Marbun, P. E. Hutajulu, G. Gultom and Y. Sitanggang, Direct Z-scheme of n-type CuS/p-type ZnS@electrospun PVP nanofiber for the highly efficient catalytic reduction of 4-nitrophenol and mixed dyes, *RSC Adv.*, 2022, **12**(25), 16165–16173.
3 G. Zhu, Q. Tang, M. Huang, J. Yang, R. Xu and J. Liu, Polyaniline nanoconical array on carbon nanofiber for supersensitive determination of nitrophenol, *Sens. Actuators, B*, 2020, **320**, 128593.
4 E. Elbayoumy, M. O. Elassi, G. M. Khairy, E. A. Moawed and M. M. aboelnga, Development of efficient fluorescent sensor for the detection of hazard aromatic nitro compounds *via* N-(1-naphthyl)ethylenediamine: experimental and DFT studies, *J. Mol. Liq.*, 2023, **391**(0167–7322), 123270.
5 B. Liang, H. Cheng, J. D. Van Nostrand, J. Ma, H. Yu, D. Kong, *et al.*, Microbial community structure and function of nitrobenzene reduction biocathode in response to carbon source switchover, *Water Res.*, 2014, **54**, 137–148.
6 M. Kulkarni and A. Chaudhari, Kinetic studies on mineralization of *p*-nitrophenol by *Pseudomonas putida* at low and high concentration, *Indian J. Chem. Technol.*, 2006, **13**(1), 60–64.
7 H. Ali and A. M. Ismail, Recyclable and Biodegradable Ag@Chitosan Nanocomposite Beads Synthesized in One-step for Catalytic Hydrogenation of 4-Nitrophenol, *J. Polym. Environ.*, 2022, **30**(8), 3379–3390.
8 M. I. Din, R. Khalid, Z. Hussain, T. Hussain, A. Mujahid, J. Najeeb, *et al.*, Nanocatalytic Assemblies for Catalytic Reduction of Nitrophenols: A Critical Review, *Crit. Rev. Anal. Chem.*, 2020, **50**, 322–338.
9 T. Rasheed, F. Nabeel, K. Rizwan, M. Bilal, T. Hussain and S. A. Shehzad, Conjugated supramolecular architectures as state-of-the-art materials in detection and remedial measures of nitro based compounds: a review, *TrAC, Trends Anal. Chem.*, 2020, **129**, 115958.
10 F. Nabeel and T. Rasheed, Rhodol-conjugated polymersomes sensor for visual and highly-sensitive detection of hydrazine in aqueous media, *J. Hazard. Mater.*, 2020, **388**, 121757.
11 T. Rasheed, C. Li, F. Nabeel, M. Qi, Y. Zhang and C. Yu, Real-time probing of mercury using an efficient 'turn-on' strategy with potential as in-field mapping kit and in live cell imaging, *New J. Chem.*, 2018, **42**(13), 10940–10946.
12 T. Rasheed, C. Li, F. Nabeel, W. Huang and Y. Zhou, Self-assembly of alternating copolymer vesicles for the highly selective, sensitive and visual detection and quantification of aqueous Hg^{2+}, *Chem. Eng. J.*, 2019, **358**, 101–109.
13 T. Rasheed, C. Li, L. Fu, F. Nabeel, C. Yu, L. Gong, *et al.*, Development and characterization of newly engineered chemosensor with intracellular monitoring potentialities and lowest detection of toxic elements, *J. Mol. Liq.*, 2018, **272**, 440–449.
14 T. Rasheed, C. Li, M. Bilal, C. Yu and H. M. N. Iqbal, Potentially toxic elements and environmentally-related pollutants recognition using colorimetric and ratiometric fluorescent probes, *Sci. Total Environ.*, 2018, **640**, 174–193.
15 T. Rasheed, C. Li, Y. Zhang, F. Nabeel, J. Peng, J. Qi, *et al.*, Rhodamine-based multianalyte colorimetric probe with potentialities as on-site assay kit and in biological systems, *Sens. Actuators, B*, 2018, **258**, 115–124.
16 M. M. Ayad, W. A. Amer and M. G. Kotp, Magnetic polyaniline-chitosan nanocomposite decorated with palladium nanoparticles for enhanced catalytic reduction of 4-nitrophenol, *Mol. Catal.*, 2017, **439**, 72–80.
17 N. Anusuya, C. Pragathiswaran and G. Thulasi. Catalytic reduction of 4-nitrophenol to 4- amino phenol by chitosan/TiO_2–Fe_2O_3 nanomaterial. in: *Materials Today: Proceedings*. 2020, pp. 3759–3763.
18 A. I. Raafat, G. A. Mahmoud and T. B. Mostafa, Efficient Catalytic Reduction of Hazardous Anthropogenic Pollutant, 4-Nitrophenol Using Radiation Synthesized (Polyvinyl Pyrrolidone/Acrylic Acid)-Silver Nanocomposite Hydrogels, *J. Inorg. Organomet. Polym. Mater.*, 2020, **30**(8), 3116–3125.
19 J. Sun, Y. Fu, G. He, X. Sun and X. Wang, Catalytic hydrogenation of nitrophenols and nitrotoluenes over a palladium/graphene nanocomposite, *Catal. Sci. Technol.*, 2014, **4**(6), 1742–1748.
20 X. Ren, L. Tang, J. Wang, E. Almatrafi, H. Feng, X. Tang, *et al.*, Highly efficient catalytic hydrogenation of nitrophenols by sewage sludge derived biochar, *Water Res.*, 2021, **201**, 117360.
21 K. Urkude, S. R. Thakare and S. Gawande, An energy efficient photocatalytic reduction of 4-nitrophenol, *J. Environ. Chem. Eng.*, 2014, **2**(1), 759–764.
22 T. Sismanoglu and S. Pura, Adsorption of aqueous nitrophenols on clinoptilolite, *Colloids Surf., A*, 2001, **180**(1–2), 1–6.
23 S. M. Tabatabaei, S. Dastmalchi, A. Mehrizad and P. Gharbani, Enhancement of 4-nitrophenol ozonation in water by nano ZnO catalyst, *Iran. J. Environ. Health Sci. Eng.*, 2011, **8**(4), 333–342.
24 M. Kulkarni and A. Chaudhari, Biodegradation of *p*-nitrophenol by P. putida, *Bioresour. Technol.*, 2006, **97**(8), 982–988.
25 F. Xie, Y. Xu, K. Xia, C. Jia and P. Zhang, Alternate pulses of ultrasound and electricity enhanced electrochemical process for *p*-nitrophenol degradation, *Ultrason. Sonochem.*, 2016, **28**, 199–206.
26 F. U. Khan, K. S. B. Asimullah, T. Kamal, A. M. Asiri, I. U. Khan, *et al.*, Novel combination of zero-valent Cu and Ag nanoparticles@cellulose acetate nanocomposite for the reduction of 4-nitro phenol, *Int. J. Biol. Macromol.*, 2017, **102**, 868–877.

27 G. Tokazhanov, S. Han and W. Lee, Enhanced catalytic reduction of *p*-nitrophenol by nano zerovalent iron - supported metal catalysts, *Catal. Commun.*, 2021, **158**, 106337.

28 E. Da'na, A. Taha and M. R. El-Aassar, Catalytic Reduction of *p*-Nitrophenol on MnO_2/Zeolite -13X Prepared with Lawsonia inermis Extract as a Stabilizing and Capping Agent, *Nanomaterials*, 2023, **13**(4), 785.

29 A. Mondal, A. Mondal, B. Adhikary and D. K. Mukherjee, Cobalt nanoparticles as reusable catalysts for reduction of 4-nitrophenol under mild conditions, *Bull. Mater. Sci.*, 2017, **40**(2), 321–328.

30 E. Elbayoumy, Y. Wang, M. A. R. Jamil, C. Trombini, M. Bando, Z. Song, *et al.*, Pd nanoparticles-loaded vinyl polymer gels: preparation, structure and catalysis, *Catalysts*, 2021, **11**(1), 137.

31 M. Ghorbanloo and H. Nosrati Fallah, Silver nanoparticle embedded anionic crosslinked copolymer hydrogels: an efficient catalyst, *J. Porous Mater.*, 2020, **27**(3), 765–777.

32 Z. H. Farooqi, S. R. Khan, T. Hussain, R. Begum, K. Ejaz, S. Majeed, *et al.*, Effect of crosslinker feed content on catalytic activity of silver nanoparticles fabricated in multiresponsive microgels, *Korean J. Chem. Eng.*, 2014, **31**(9), 1674–1680.

33 R. R. Palem, S. D. Ganesh, N. Saha, J. Kronek and P. Sáha, Green' synthesis of silver polymer Nanocomposites of poly (2-isopropenyl-2- oxazoline-*co*-*N*-vinylpyrrolidone) and its catalytic activity, *J. Polym. Res.*, 2018, **25**(7), 152.

34 S. Varshney, R. Bar-Ziv and T. Zidki, On the Remarkable Performance of Silver-based Alloy Nanoparticles in 4-Nitrophenol Catalytic Reduction, *ChemCatChem*, 2020, **12**(18), 4680–4688.

35 S. R. Khan, Z. H. Farooqi, M. Ajmal, M. Siddiq and A. Khan, Synthesis, Characterization, and Silver Nanoparticles Fabrication in *N*-isopropylacrylamide-Based Polymer Microgels for Rapid Degradation of *p*-Nitrophenol, *J. Dispersion Sci. Technol.*, 2013, **34**(10), 1324–1333.

36 Y. Lu, Y. Shi, Y. Wang, J. Cao, J. Wang, Y. Zheng, *et al.*, A defect-enriched PdMo bimetallene for ethanol oxidation reaction and 4-nitrophenol reduction, *Chem. Commun.*, 2024, **60**(24), 3323–3326.

37 F. Wei, M. Luo, J. Lan, F. Xie, L. Cai, T. S. Chan, *et al.*, Pd Atomic Engineering of Nanoporous Ni/NiO for Efficient Nitrophenol Hydrogenation Reaction, *ACS Appl. Mater. Interfaces*, 2023, **15**(22), 26746–26754.

38 Y. Wang, Y. Lu, Y. Shi, J. Wang, Y. Zheng, J. Pan, *et al.*, Realizing highly-efficient urea oxidation *via* decreasing the energy barrier of deprotonation over regulated electronic structure of Co doped $Ni(OH)_2$, *Appl. Surf. Sci.*, 2023, **640**, 158391.

39 L. Que, L. Lu, Y. Xu, X. Xu, M. Zhu, J. Pan, *et al.*, The Ni^{2+}-$LaNiO_3$/CdS hollow core–shell heterojunction towards enhanced visible light overall water splitting H_2 evolution *via* HER/OER synergism of Ni^{2+}/Ov, *Chem. Eng. J.*, 2023, **469**, 143902.

40 P. Jing, C. He, S. Huang, H. Li, J. Liu, Y. Cui, *et al.*, 2D Z-scheme heterojunction and oxygen deficiency synergistically boosting the photocatalytic activity of a layered $BaTiO_3$/$BiOIO_3$ composite, *Appl. Mater. Today*, 2022, **29**, 101574.

41 P. Zhang, Y. shi, Y. Zhang, S. Feng, L. Shi, J. Pan, *et al.*, Self-cleaning transparent pn junction in $CuAlO_2$/WO_3 *via* high entropy perovskite oxide La(Cu0.2Cr0.2Ni0.2Fe0.2Co0.2)O_3 transition layer for enhanced photovoltaic conversion, *Chem. Eng. J.*, 2024, **487**, 150727.

42 S. Shen, H. Zhang, K. Song, Z. Wang, T. Shang, A. Gao, *et al.*, Multi-d Electron Synergy in LaNi1-xCoxRu Intermetallics Boosts Electrocatalytic Hydrogen Evolution, *Angew. Chem., Int. Ed.*, 2024, **63**(1), e202315340.

43 F. Laghrib, H. Houcini, F. Khalil, A. Liba, M. Bakasse, S. Lahrich, *et al.*, Synthesis of Silver Nanoparticles Using Chitosan as Stabilizer Agent: Application towards Electrocatalytical Reduction of *p*-Nitrophenol, *ChemistrySelect*, 2020, **5**(3), 1220–1227.

44 A. Zhou, J. Li, G. Wang and Q. Xu, Preparation of Ag/ZrGP nanocomposites with enhanced catalytic activity for catalytic reduction of 4-nitrophenol, *Appl. Surf. Sci.*, 2020, **506**, 144570.

45 H. Gebru, S. Cui, Z. Li, X. Wang, X. Pan, J. Liu, *et al.*, Facile pH-Dependent Synthesis and Characterization of Catechol Stabilized Silver Nanoparticles for Catalytic Reduction of 4-Nitrophenol, *Catal. Lett.*, 2017, **147**(8), 2134–2143.

46 M. Maham, M. Nasrollahzadeh and S. Mohammad Sajadi, Facile synthesis of Ag/ZrO_2 nanocomposite as a recyclable catalyst for the treatment of environmental pollutants, *Composites, Part B*, 2020, **185**, 107783.

47 M. A. Diab, N. A. El-Ghamaz, F. S. Mohamed and E. M. El-Bayoumy, Conducting polymers VIII: Optical and electrical conductivity of poly(bis-*m*-phenylenediaminosulphoxide), *Polym. Test.*, 2017, **63**, 440–447.

48 Z. H. Farooqi, N. Tariq, R. Begum, S. R. Khan, Z. I. Qbal and A. Khan, Fabrication of silver nanoparticles in poly(*N*-isopropylacrylamide-*co*-allylacetic acid) microgels for catalytic reduction of nitroarenes, *Turk. J. Chem.*, 2015, **39**(3), 576–588.

49 R. Begum, Z. H. Farooqi, E. Ahmed, K. Naseem, S. Ashraf, A. Sharif, *et al.*, Catalytic reduction of 4-nitrophenol using silver nanoparticles-engineered poly(*N*-isopropylacrylamide-*co*-acrylamide) hybrid microgels, *Appl. Organomet. Chem.*, 2017, **31**(2), e3563.

50 Z. H. Farooqi, S. R. Khan, R. Begum, F. Kanwal, A. Sharif, E. Ahmed, *et al.*, Effect of acrylic acid feed contents of microgels on catalytic activity of silver nanoparticles fabricated hybrid microgels, *Turk. J. Chem.*, 2015, **39**(1), 96–107.

51 M. Ajmal, S. Demirci, M. Siddiq, N. Aktas and N. Sahiner, Simultaneous catalytic degradation/reduction of multiple organic compounds by modifiable p(methacrylic acid-*co*-acrylonitrile)-M (M: Cu, Co) microgel catalyst composites, *New J. Chem.*, 2016, **40**(2), 1485–1496.

52 O. Hazer, C. Soykan and S. Kartal, Synthesis and swelling behavior analysis of poly(acrylamidoxime-*co*-2- acrylamido-2-methylpropane sulfonic acid) hydrogels, *J. Macromol. Sci., Part A: Pure Appl.Chem.*, 2008, **45**(1), 45–51.

53 Z. He, H. Liu, G. Yang, C. Jiang, M. Ji, J. Yu, *et al.*, Cyclization mechanism and kinetics of poly(acrylonitrile-*co*-2-acrylamido-2-methylpropane sulfonic acid) copolymer investigated by FTIR spectroscopy, *Polym. Test.*, 2021, **93**, 106969.

54 J. R. Ebdon, T. N. Huckerby and T. C. Hunter, Free-radical aqueous slurry polymerizations of acrylonitrile: 1. end-groups and other minor structures in polyacrylonitriles initiated by ammonium persulfate/sodium metabisulfite, *Polymer*, 1994, **35**(2), 250–256.

55 A. Haleem, S. B. Syaal, M. Ajmal, J. Ambreen, S. Rauf, N. Ali, *et al.*, Silver and palladium nanoparticle embedded poly(*n*-isopropylacrylamide-*co*-2-acrylamido-2-methylpropane sulfonic acid) hybrid microgel catalyst with pH and temperature dependent catalytic activity, *Korean J. Chem. Eng.*, 2020, **37**(4), 614–622.

56 A. M. Atta, M. Akel, R. A. Elghazawy and M. Alaa, Characterization of modified styrene-*co*-2-acrylamido-2-methylpropane sulfonic acid magnetite nanoparticles, *Polym. Sci., Ser. A*, 2013, **55**(5), 327–335.

57 P. Das, D. Dutta, A. Sarkar, R. Dubey and A. Puzari, Acrylonitrile Adducts: An Efficient Adsorbent Media for Removal of Iron from Water, *ChemistrySelect*, 2022, **7**(41), e202203048.

58 A. M. Atta, S. A. Sayed, A. B. Farag, H. S. Ismail, Z. M. Mohamed and A. M. Eraky, Application of crosslinked acrylamidoxime/2-acrylamido-2-methylpropane sulfonic acid copolymer in wastewater treatment, *J. Dispersion Sci. Technol.*, 2011, **32**(9), 1285–1295.

59 P. K. Dara, R. Mahadevan, P. A. Digita, S. Visnuvinayagam, L. R. G. Kumar and S. Mathew, nthesis and biochemical characterization of silver nanoparticles grafted chitosan (Chi-Ag-NPs): *in vitro* studies on antioxidant and antibacterial applications, *SN Appl. Sci.*, 2020, **2**(4), 665.

60 E. Elbayoumy, N. A. El-Ghamaz, F. S. Mohamed, M. A. Diab and T. Nakano, Dielectric permittivity, AC electrical conductivity and conduction mechanism of high crosslinked-vinyl polymers and their $Pd(OAc)_2$ composites, *Polymers*, 2021, **13**(17), 3005.

61 L. Zhou, Y. Wang, Q. Huang and J. Cai, Thermogravimetric characteristics and kinetic of plastic and biomass blends co-pyrolysis, *Fuel Process. Technol.*, 2006, **87**(11), 963–969.

62 E. Elbayoumy, M. Elhendawy, M. M. Gaafar, E. A. Moawed and M. M. aboelnga, Novel fluorescent sensor based on triazole-pyridine derivative for selective detection of mercury (II) ions in different real water samples: experimental and DFT calculations, *J. Mol. Liq.*, 2024, **401**, 124589.

63 N. A. El-Ghamaz, T. S. Ahmed and D. A. Salama, Optical, dielectrical properties and conduction mechanism of copolymer (*N*,*N*′-bissulphinyl-*m*-benzenediamine-*p*-phenylenediamine), *Eur. Polym. J.*, 2017, **93**, 8–20.

64 H. S. Mahmood and M. K. Jawad. Antibacterial activity of chitosan/PAN blend prepared at different ratios, in *AIP Conference Proceedings*. 2019, p. 020078.

65 A. M. Atta, G. A. El-Mahdy, H. A. Al-Lohedan and A. O. Ezzat, Synthesis and application of hybrid polymer composites based on silver nanoparticles as corrosion protection for line pipe steel, *Molecules*, 2014, **19**(5), 6246–6262.

66 M. M. Rahman, T. Demirel, K. Ş. Tunçel and I. Karacan, The effect of the ammonium persulfate and a multi-step annealing approach during thermal stabilization of polyacrylonitrile multifilament prior to carbonization, *J. Mater. Sci.*, 2021, **56**(26), 14844–14865.

67 B. D. Zdravkov, J. J. Čermák, M. Šefara and J. Janků, Pore classification in the characterization of porous materials: a perspective, *Cent. Eur. J. Chem.*, 2007, **5**(2), 385–395.

68 T. B. Nguyen, C. P. Huang and R. an Doong, Enhanced catalytic reduction of nitrophenols by sodium borohydride over highly recyclable Au@graphitic carbon nitride nanocomposites, *Appl. Catal., B*, 2019, **240**, 337–347.

69 P. Pootawang and S. Y. Lee, Rapid synthesis of Ag nanoparticles-embedded mesoporous silica *via* solution plasma and its catalysis for 4-nitrophenol reduction, *Mater. Lett.*, 2012, **80**, 1–4.

70 S. Mehmood, N. K. Janjua, F. Saira and H. Fenniri, AuCu@Pt nanoalloys for catalytic application in reduction of 4-nitrophenol, *J. Spectrosc.*, 2016, **2016**, 6210794.

71 T. K. Das, S. Ganguly, S. Remanan, S. Ghosh and N. C. Das, Mussel-inspired Ag/poly(norepinephrine)/MnO_2 heterogeneous nanocatalyst for efficient reduction of 4-nitrophenol and 4-nitroaniline: an alternative approach, *Res. Chem. Intermed.*, 2020, **46**(7), 3629–3650.

72 K. Sravanthi, D. Ayodhya and P. Y. Swamy, Green synthesis, characterization and catalytic activity of 4-nitrophenol reduction and formation of benzimidazoles using bentonite supported zero valent iron nanoparticles, *Mater. Sci. Energy Technol.*, 2019, **2**(2), 298–307.

73 K. Dânoun, R. Tabit, A. Laghzizil and M. Zahouily, A novel approach for the synthesis of nanostructured Ag_3PO_4 from phosphate rock: high catalytic and antibacterial activities, *BMC Chem.*, 2021, **15**(1), 42.

74 T. A. Revathy, S. Dhanavel, T. Sivaranjani, V. Narayanan, T. Maiyalagan and A. Stephen, Highly active graphene-supported palladium-nickel alloy nanoparticles for catalytic reduction of 4-nitrophenol, *Appl. Surf. Sci.*, 2018, **449**, 764–771.

75 S. K. Ghosh, M. Mandal, S. Kundu, S. Nath and T. Pal, Bimetallic Pt-Ni nanoparticles can catalyze reduction of aromatic nitro compounds by sodium borohydride in aqueous solution, *Appl. Catal., A*, 2004, **268**(1–2), 61–66.

76 S. Chairam, W. Konkamdee and R. Parakhun, Starch-supported gold nanoparticles and their use in 4-nitrophenol reduction Starch-supported gold nanoparticles in 4-nitrophenol reduction, *J. Saudi Chem. Soc.*, 2017, **21**(6), 656–663.